The turbulence dissipation constant is not universal because of its universal dependence on large-scale flow topology

N. Mazellier
Turbulence, Mixing and Flow Control Group, Department of Aeronautics, Imperial College London, London, SW7 2BY, United Kingdom

J. C. Vassilicos
Turbulence, Mixing and Flow Control Group, Department of Aeronautics and Institute for Mathematical Sciences, Imperial College London, London, SW7 2BY, United Kingdom

(Received 15 August 2007; accepted 24 November 2007; published online 23 January 2008)

The dimensionless dissipation rate constant C_ϵ of homogeneous isotropic turbulence is such that $C_\epsilon = f(\log \mathrm{Re}_\lambda) C_s'^3$, where $f(\log \mathrm{Re}_\lambda)$ is a dimensionless function of $\log \mathrm{Re}_\lambda$ which tends to 0.26 (by extrapolation) in the limit where $\log \mathrm{Re}_\lambda \gg 1$ (as opposed to just $\mathrm{Re}_\lambda \gg 1$) if the assumption is made that a finite such limit exists. The dimensionless number C_s' reflects the number of large-scale eddies and is therefore nonuniversal. The nonuniversal asymptotic values of C_ϵ stem, therefore, from its universal dependence on C_s'. The Reynolds number dependence of C_ϵ at values of $\log \mathrm{Re}_\lambda$ close to and not much larger than 1 is primarily governed by the slow growth (with Reynolds number) of the range of viscous scales of the turbulence. An eventual Reynolds number independence of C_ϵ can be achieved, in principle, by an eventual balance between this slow growth and the increasing non-Gaussianity of the small scales. The turbulence is characterized by five length-scales in the following order of increasing magnitude: the Kolmogorov microscale η, the inner cutoff scale $\eta_* \approx \eta(7.8+9.1 \log \mathrm{Re}_\lambda)$, the Taylor microscale $\lambda \sim \mathrm{Re}_\lambda^{1/2} \eta$, the voids length scale $\lambda_v \sim \mathrm{Re}_\lambda^{1/3} \lambda$, and the integral length scale $L \sim \mathrm{Re}_\lambda^{2/3} \lambda_v$. © *2008 American Institute of Physics*.
[DOI: 10.1063/1.2832778]

I. INTRODUCTION

In one of the most important papers ever written on fully developed fluid turbulence, Taylor[1] proved that, if the turbulence is isotropic, the kinetic energy dissipation per unit mass, ϵ, is equal to $15\nu u'^2/\lambda^2$, where ν is the fluid's kinematic viscosity, u' is the rms velocity of the turbulence, and λ is the Taylor microscale. In that same paper, Taylor[1] introduced and tested experimentally a relation which is now widely regarded as the cornerstone property of fully developed turbulence, $\epsilon = C_\epsilon u'^3/L$, where the dimensionless constant C_ϵ is independent of Reynolds number in the limit of high Reynolds number $\mathrm{Re} \equiv u'L/\nu$, where L is the longitudinal integral length-scale of the turbulence. Since then, a multitude of laboratory experiments and numerical simulations[2–7] concerned with isotropic homogeneous turbulence seem to confirm that C_ϵ is independent of Reynolds number in the limit of high Reynolds number, but are not conclusive as to whether C_ϵ is universal at such high Reynolds number values. In fact, the high Reynolds number values of C_ϵ seem to differ from flow to flow. At lower Reynolds numbers where C_ϵ is Reynolds number dependent, C_ϵ is, as one might expect, quite clearly not universal.

An interesting observation about the Taylor microscale λ was made by Rice[8,9] and Liepmann:[10,11] the average distance between consecutive zero-crossings of a statistically stationary stochastic function $u(x)$ is equal to $\pi\langle u^2\rangle^{1/2}/\langle (du/dx)^2\rangle^{1/2}$ if $u(x)$ and du/dx have Gaussian distributions centered around zero and are statistically independent (see Appendix). Sreenivasan *et al.*[12] demonstrated that this relation is a good approximation for many different turbulence signals in many different turbulent flows (longitudinal velocity fluctuations in boundary layers and a wake, wall shear stress in a channel and temperature derivatives in a heated boundary layer) and suggested, as a result, that the assumption of Gaussianity may, in fact, not be necessary. If $u(x)$ is taken to be a longitudinal velocity fluctuation component, then $\langle u^2\rangle^{1/2}/\langle (du/dx)^2\rangle^{1/2} = u'/\langle (du/dx)^2\rangle^{1/2}$ is the Taylor microscale λ in $\epsilon = 15\nu u'^2/\lambda^2$. This Taylor microscale multiplied by π is therefore equal to the average distance $\bar{l}$ between consecutive zero-crossings of $u(x)$, i.e., points x where $u(x)=0$.

Sreenivasan and co-workers[13] and Davila and Vassilicos[14] went one step further: they demonstrated that the number density n_s of zero-crossings of the longitudinal velocity fluctuation component $u(x)$ is a power-law function of L/η_c, where $2\pi/\eta_c$ is the filter wavenumber of a low-pass filter applied on $u(x)$. Specifically, in terms of a dimensionless constant C_s', Davila and Vassilicos[14] found that

$$n_s(L/\eta_c) = \frac{C_s'}{L}(L/\eta_c)^{2/3} \tag{1}$$

in wind-tunnel grid turbulence at various Reynolds numbers and for various values of η_c. It may be interesting to note that the power law (1) has been mathematically proven to hold by Orey[15] for Gaussian stochastic functions with a Fourier power spectrum that has a power-law shape with a $-5/3$ exponent. Turbulent velocity component fluctuations do have such spectra but do not have Gaussian velocity derivatives. It

TABLE I. Round air jet data used here. They were obtained by hot-wire anemometry from the jet's centerline by Mazellier (Ref. 17) (first line) and by Naert and Baudet (Ref. 18) (second line). In both cases, the hot wire diameter was of 3 μm, the sensing length to diameter ratio was 120 for Mazellier and 330 for Naert and Baudet, and spatial velocity fluctuations were derived using the local Taylor hypothesis as described in Kahalerras *et al.* (Ref. 19). The spatial hot-wire resolution ranges between 5η at $x=60d$ and 1.8η at $x=110d$ in the case of Mazellier's (Ref. 17) data and is 7.7 and 11.3η, respectively, for the data of Naert and Baudet (Ref. 18). The frequency resolution ranges between 7.2 and 39.3 Kolmogorov frequencies from $x=60$ to $x=110d$ in the case of Mazellier's (Ref. 17) data and is 3.8 and 5.7 Kolmogorov frequencies, respectively, for the data of Naert and Baudet (Ref. 18).

Nozzle diameter	Exit velocity	Streamwise distance from nozzle	Turbulence intensity	Re_λ	L
$d=2.25$ cm	50 m/s	$50d$, $60d$, $70d$, $80d$, $90d$, $100d$, $110d$	26%	380	4.7 cm to 10.3 cm
$d=5$ cm	18 m/s and 30 m/s	$50d$	28% and 27%	390 and 490	12 cm and 10.4 cm

is interesting that the stagnation points of turbulent velocity signals have scaling properties which are not affected by the non-Gaussianity of velocity derivatives.

In this paper we confirm and extend the observation of Davila and Vassilicos[14] and then combine it with the aforementioned Taylor and Rice–Liepmann results to estimate the turbulence dissipation constant C_ϵ.

II. THE DISSIPATION CONSTANT C_ϵ IS PROPORTIONAL TO THE THIRD POWER OF THE NUMBER C_s' OF LARGE-SCALE EDDIES: $C_\epsilon = f(\log \mathrm{Re}_\lambda) C_s'^3$

We start by confirming Eq. (1) by testing it for a wide range of values of η_c between η and L in two different round jet flows (see Table I), in "chunk" turbulence at the S1 wind tunnel of Modane and in wind tunnel turbulence generated by various grids (see Tables II and III): two different classical grids (regular grids made of equidistant identical square bars), one fractal cross grid, and one fractal I grid (see Hurst and Vassilicos[16] for a detailed description of fractal grids, including the ones used here, and the turbulence they generate). All data are of $u(x)$ on the centerline of each flow. Some of the results are plotted in Fig. 1. For this figure, $n_s(L/\eta_c)$ has been obtained by low-pass filtering the signal $u(x)$ using a fifth order filter with filter wavenumber $2\pi/\eta_c$ and then counting zero-crossings of the filtered signal (we checked that results do not change with higher order filters); $\bar{l}$ has been obtained independently by averaging distances between consecutive zero-crossings of the unfiltered signal. For this and all other figures, the longitudinal integral length-scale L has been calculated by integrating the autocorrelation function of $u(x)$. Furthermore, the lengths of the data sets used to calculate $n_s(L/\eta_c)$ and $\bar{l}$ in this paper are long enough for statistical convergence of all quantities calculated here, something which we have systematically checked. They are $1.4\times10^4 L$ for fractal I grid turbulence, $9\times10^4 L$ for fractal cross grid turbulence, about $10^4 L$ for the Modane data, $8\times10^4 L$ and $4\times10^4 L$ for the larger nozzle jet at $\mathrm{Re}_\lambda \equiv u'\lambda/\nu = 390$ and 490, respectively, from $2.5\times10^4 L$ to $5\times10^3 L$ for the smaller nozzle jet from $50d$ to $110d$, and between $10^4 L$ and $6\times10^4 L$ for classical grid turbulence (see

TABLE II. (i) Wind tunnel grid-generated (except in Modane) turbulence data used here. They were obtained by hot wire anemometry from the tunnel's centerline by Mazellier (Ref. 17) with a classical grid (first line), by the current authors with a classical grid (second line) and a fractal I grid (Ref. 16) corresponding to Fig. 17e in Hurst and Vassilicos (Ref. 16) (fourth line), by Hurst and Vassilicos (Ref. 16) with a fractal cross grid corresponding to Fig. 3(c) in their paper (third line) and by Malecot and Gagne (Refs. 19 and 20) in wind tunnel S1 at Modane (fifth line). The Modane data are of so-called "chunk" turbulence (Refs. 19 and 20) which is not grid-generated. The section size and length are the wind tunnel test section's. The mesh size is the mesh size M of the classical grid (square bars) or the effective mesh size M_{eff} of the fractal grid (Ref. 16). The blockade ratio is that of the grid. We used the same hot wire as Hurst and Vassilicos (Ref. 16), i.e., 5 μm wire diameter and sensing length to diameter ratio of 200. Mazellier (Ref. 17) and Malecot and Gagne (Refs. 19 and 20) used a 3 μm diameter wire with a sensing length to diameter ratio of 120. The spatial hot-wire resolution ranges between 1.3 and 3.6η for Mazellier's (Ref. 17) data, between 2.1 and 3.8η for the data of Hurst and Vassilicos (Ref. 16) between 1.5 and 6η for our data and is about 1.5η for the Modane data. The frequency resolution varies from 5 to 90 Kolmogorov frequencies for Mazellier's (Ref. 17) from 3 to 5 Kolmogorov frequencies for the data of Hurst and Vassilicos (Ref. 16) and is around 2 Kolmogorov frequencies for the Modane data. For our data, it ranges between 5 and 100 Kolmogorov frequencies. We used a DISA 55M10 anemometer which has a 50 kHz frequency response with the wire we used, well above the highest resolvable frequencies for our wire and flow speeds. Our acquisition card is NI9215 (USB NI Compact DAQ) with 16 bit resolution. Our signal to noise ratio ranges between 36 and 48 dB. Our calibration procedure was made using a Pitot tube before and after each run and King's law was used for the conversion from voltage to velocity. We also monitored the temperature during measurements to make sure that no compensation for temperature drift was needed. The local Taylor hypothesis described in Kahaleras *et al.* (Ref. 19) was used to derive spatial velocity fluctuations in all the flows of this table.

	Section size	Section length	Mesh size	Blockade ratio
Classical grid	75 cm×75 cm	4 m	$M=7.5$ cm	34%
Classical grid	46 cm×46 cm	5 m	$M=3.2$ cm	34%
Fractal cross grid	91 cm×91 cm	5.4 m	$M_{\mathrm{eff}}=5.7$ cm	21%
Fractal I grid	46 cm×46 cm	5 m	$M_{\mathrm{eff}}=3.55$ cm	25%
Modane	24 m diameter	N.A.	N.A.	N.A.

TABLE III. Wind tunnel turbulence data used here, presented in the same order as in Table II. See caption of Table II for details.

Mean inlet velocity	Streamwise distance from grid	Turbulence intensity	Re_λ	L
9 and 16 m/s	$35M$, $38M$, and $42M$	3.3%	130 and 180	6.0 to 6.6 cm
2.5, 5, and 10 m/s	$40M$	2.5%	39, 56, and 82	3.2 to 2.2 cm
6, 8, and 16 m/s	$75M_{\text{eff}}$	2.7%	91, 111, and 189	5.8 cm
10 m/s	$65M_{\text{eff}}$, $72M_{\text{eff}}$, and $83M_{\text{eff}}$	7%	238	6.3 cm
20, 20.7, and 20.8 m/s	N.A.	7.3%	1918, 2263, and 2486	1.6 to 2.1 m

Tables I–III for details on these data and related notation). High frequency noise generates its own stagnation points and we took care in removing them by filtering out the frequencies where the noise dominates the power spectrum. We verified our procedures on known functions such as sine waves and chirps with various degrees of added noise.

We find, in all turbulent flows tried here, that an inner cutoff scale η_* exists such that $\bar{l}n_s(L/\eta_c) \approx 1$ for $\eta_* \gtrsim \eta_c$, and that Eq. (1) holds in the range of scales η_c between the inner cutoff scale η_* and L. This means that η_* is the inner cutoff scale below which one does not find new stagnation points. Furthermore, the dimensionless constant C_s' is therefore well-defined in the range of scales η_c between the inner cutoff scale η_* and L but turns out to be different for different turbulent flows. C_s' calculated as in Fig. 1 is only weakly dependent on streamwise distance from the nozzle in the centerline round jet turbulence and also weakly dependent on streamwise distance from the grid in the centerline wind tunnel turbulence (see Fig. 3 below). This holds for all grids, the classical, the fractal cross and the fractal I grids. However, as can be seen in Fig. 1, C_s' differs from flow to flow; for example, it is significantly larger for classical grid turbulence than for jet turbulence.

It is important to realize that C_s' is a dimensionless constant characterizing the largest eddies of the turbulence. Indeed, Fig. 1 demonstrates that the value of C_s' can be obtained unaltered after low-pass filtering a turbulence data set irrespective of the filter size η_c, as long as η_c is between η_* and L.

This observation is important because the average distance between consecutive zero-crossings is $n_s^{-1}(L/\eta_*)$. Following Rice[8,9] and Liepmann,[10,11] we may write $n_s^{-1}(L/\eta_*) = \pi\lambda$. However, we define the constant B by $n_s^{-1}(L/\eta_*) = B\lambda$ in the expectation that the proportionality $n_s^{-1}(L/\eta_*) \sim \lambda$ may hold in turbulent flows even though they are non-Gaussian but that the constant B may differ from π as a result of this non-Gaussianity (see Appendix). Defining the dimensionless constant $A \equiv \eta_*/\eta$, where $\eta = (\nu^3/\epsilon)^{1/4}$ is the Kolmogorov microscale, setting $\eta_c = \eta_*$ in Eq. (1) and using it in conjunction with $n_s^{-1}(L/\eta_*) = B\lambda$, Taylor's relation $\epsilon = 15\nu u'^2/\lambda^2$ and $\epsilon = C_\epsilon u'^3/L$, it then follows that

$$C_\epsilon = (15B^2)^{3/2}\left(\frac{C_s'}{A^{2/3}}\right)^3. \tag{2}$$

We define $K \equiv (15\pi^2)^{3/2} \approx 1801.3$. We also introduce $B = C\pi$ so that Eq. (2) may be recast as $C_\epsilon = K(CC_s'/A^{2/3})^3$.

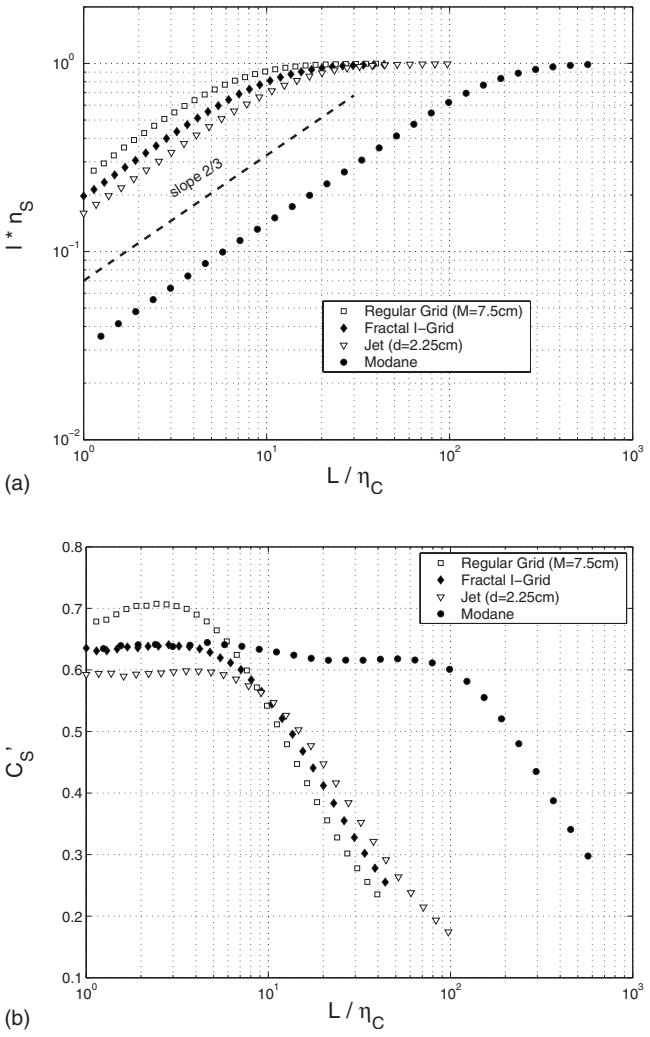

FIG. 1. Plots of (a) $\log(\bar{l}n_s)$ vs $\log(L/\eta_c)$ (to the left) and of (b) $C_s' = n_s L(L/\eta_c)^{-2/3}$ vs $\log(L/\eta_c)$ (to the right) for longitudinal velocity fluctuations $u(x)$ obtained on the centerline of four different turbulent flows: a round air jet with nozzle diameter $d=2.25$ cm (streamwise distance from the nozzle $50d$, but we have confirmed the 2/3 power law with data from $60d$, $70d$, $80d$, $90d$, $100d$, and $110d$); turbulence generated by a classical grid in a square 75 cm × 75 cm wind tunnel (mean inlet velocity 9 m/s and streamwise distance from grid $42M$, but we have confirmed the 2/3 power law with data from $35M$ and $38M$ and mean inlet velocities 9 and 16 m/s); turbulence generated by a fractal I grid (streamwise distance from grid $83M_{\text{eff}}$, but we have confirmed the 2/3 power law with data from $65M_{\text{eff}}$ and $72M_{\text{eff}}$); and "chunk" turbulence in the S1 wind tunnel of Modane ($Re_\lambda = 2263$, but we have confirmed the 2/3 power law with the other two Modane data sets). Summary descriptions of these data can be found in Tables I–III.

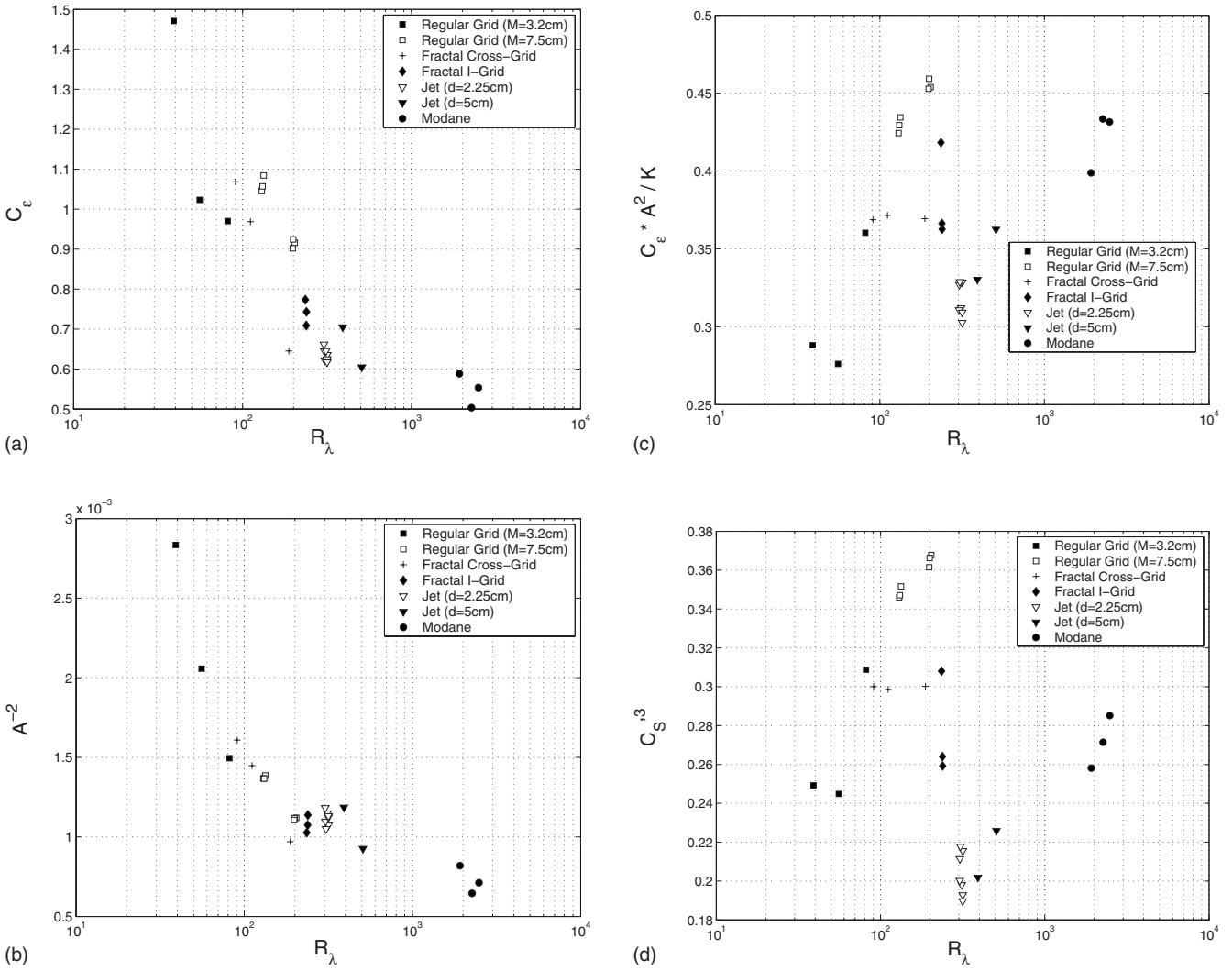

FIG. 2. Lin-log plots of C_ϵ, A^{-2}, $C_\epsilon A^2/K$, $C_s'^3$, and $K(C_s'/A^{2/3})^3$ as functions of Re_λ. To calculate C_ϵ we use $C_\epsilon u'^3/L=15\nu\langle(du/dx)^2\rangle$. To calculate C_s' we use $C_s'=L(L/\eta_*)^{-2/3}n_s(L/\eta_*)$ with $\eta_*=A\eta$, where A is estimated as described in the main text and η is calculated from $\eta=(\nu^3/\epsilon)^{1/4}$ with $\epsilon=15\nu\langle(du/dx)^2\rangle$. The constant $K=(15\pi^2)^{3/2}\approx 1801.3$.

Note that, to obtain this equation, we do not need to assume that C_ϵ is independent of Reynolds number. As C_s' is Reynolds number independent, any Reynolds number dependence of C_ϵ will have to come from Reynolds number dependencies of A and/or B.

Equation (2) is a remarkable relation because it suggests that the small-scale dissipation rate, represented by the dimensionless number C_ϵ, is directly and strongly dependent ($C_\epsilon \propto C_s'^3$) on the large-scale dimensionless number C_s'. This large-scale number is something like a number of large-scale eddies within an integral scale. Modify this number and you modify the normalized turbulence dissipation rate C_ϵ. This may be the reason why the high Reynolds number values of C_ϵ obtained in various laboratory and numerical experiments[2–7] seem to differ from turbulent flow to turbulent flow. In Fig. 2 we plot C_ϵ as a function of Re_λ for a total of 27 different $u(x)$ data sets from 7 different turbulent flows (Tables I–III).

It is clear from Fig. 2 that C_ϵ varies significantly from flow to flow and also with Reynolds number. A plot of C_s' calculated from Eq. (1) with $\eta_c=\eta_*$, i.e., $C_s'=n_s(L/\eta_*)L(L/\eta_*)^{-2/3}$, is given in Fig. 3 as a function of Re_λ for the same turbulence data sets. A calculation of η_* is required prior to that of C_s', and this is achieved by fitting a straight line of 2/3 slope to the L/η_c-dependent side of the data in Fig. 1(a) and finding the intersection of this line with the horizontal line $\log(\bar{l}n_s)=0$ in that figure. We estimate $\log(L/\eta_*)$ from the value of $\log(L/\eta_c)$ where this intersection occurs and plot the resulting $A=\eta_*/\eta$ as a function of Re_λ in Fig. 3. We find that $A\approx 7.8+9.1\log \mathrm{Re}_\lambda$ is a reasonable fit for all 27 data sets from our 7 different turbulent flows in the range of Reynolds numbers covered. [Other functional forms could be used to fit these data, such as $a_1(1+a_2\mathrm{Re}_\lambda^b)$, but they either lead to significantly worse fits if b is constrained to be positive, or to a satisfactory fit but with a negative value of b which, as we explain in the paragraph which contains Eq. (3), runs counter to the dual requirement that C_ϵ should be finite and the small-scale turbulence increasingly non-Gaussian in the limit $\mathrm{Re}_\lambda\to\infty$.] This

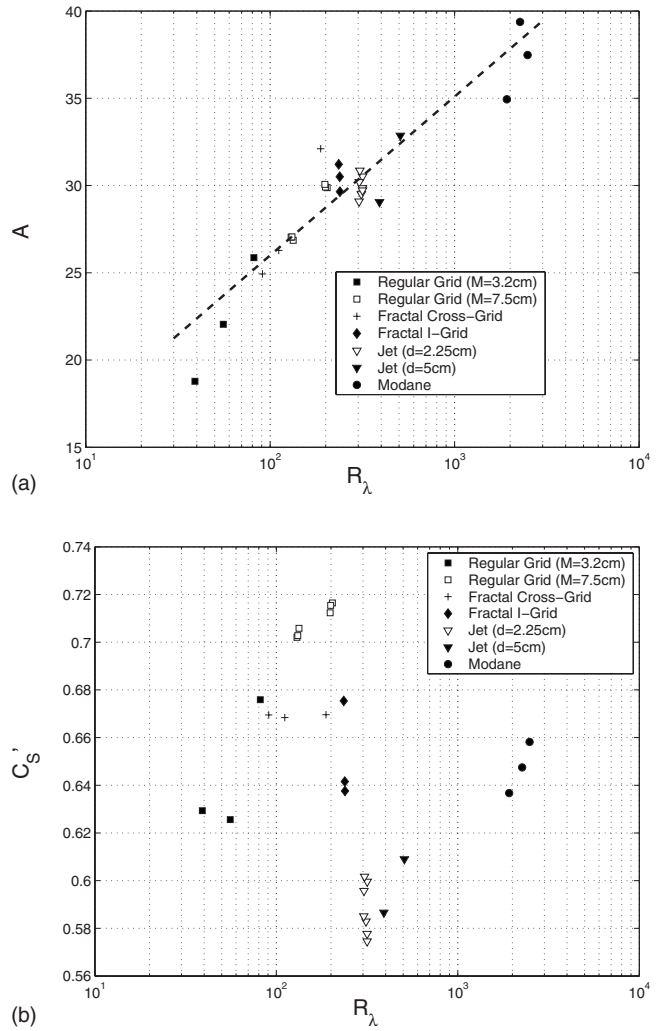

FIG. 3. Lin-log plots of A and of $C_s'=L(L/\eta_*)^{-2/3}n_s(L/\eta_*)$ as functions of Re_λ. The dotted line in the plot of A vs Re_λ is $A=7.8+9.1\log \mathrm{Re}_\lambda$. Explanations for how A and C_s' are calculated are given in the main text and the caption of Fig. 2.

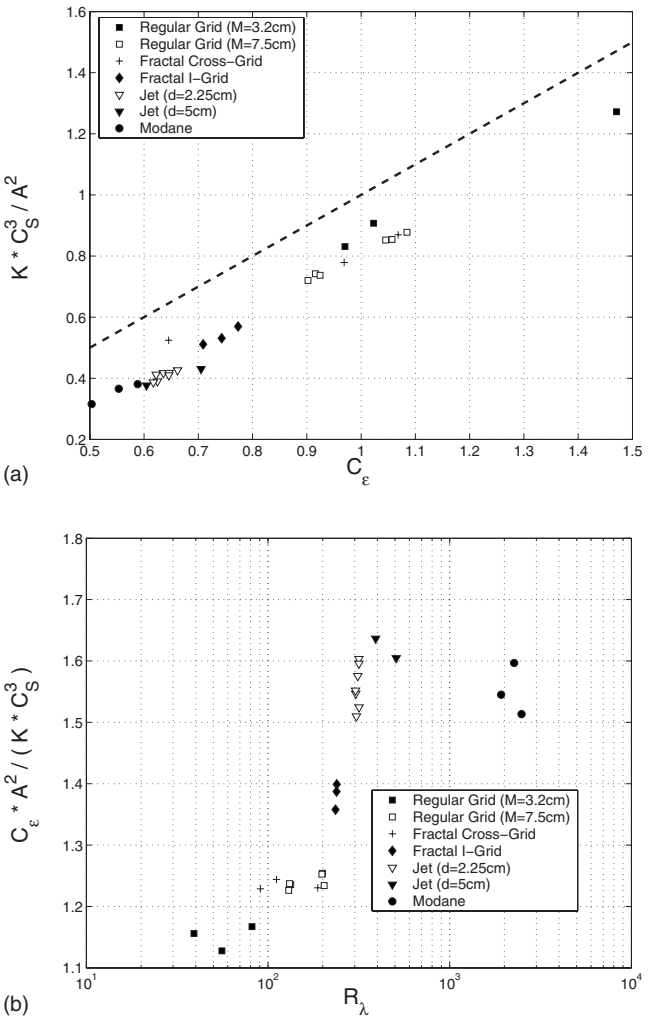

FIG. 4. Plots of $K(C_s'/A^{2/3})^3$ vs C_ϵ and of $C_\epsilon/K(C_s'/A^{2/3})^3$ as a function of $\log \mathrm{Re}_\lambda$. Explanations for how A and C_s' are calculated are given in the main text and the caption of Fig. 2. The dotted line in the top plot is $K(C_s'/A^{2/3})^3=C_\epsilon$ and $K=(15\pi^2)^{3/2}\approx 1801.3$.

means that the inner length-scale η_* scales as the Kolmogorov microscale η modulo a logarithmic correction in Reynolds number, at least in the range of Re_λ between about 60 and $O(1000)$.

This monotonic increase of A with Reynolds number seems to account for much of the Reynolds number dependence of C_ϵ in Fig. 2. We plot A^{-2} versus Re_λ in that same figure for comparison with the plot of C_ϵ versus Re_λ. In agreement with Eq. (2) which implies $C_\epsilon \sim A^{-2}$, the two Reynolds number dependencies look similar. Hence, Eq. (2) can also account for much of the Reynolds number dependence of C_ϵ via its dependence on the microscale dimensionless number A. Plotting $C_\epsilon A^2$ versus Re_λ (see Fig. 2) does remove the systematically monotonic variability with Re_λ but keeps a very significant scatter (of the order of 30%) around a mean value which appears independent of Re_λ. Plotting $C_s'^3$ versus Re_λ as part of Fig. 2 for comparison with the plot of $C_\epsilon A^2$ versus Re_λ reveals an equally significant and very similar scatter in qualitative agreement with Eq. (2) which implies $C_\epsilon A^2 \sim C_s'^3$.

The variations of C_s' from flow to flow and with Reynolds number (see Fig. 3) may not be as significant as those of C_ϵ, but those of $C_s'^3$ from flow to flow are definitely as significant as those of $C_\epsilon A^2$ from flow to flow (Fig. 2). In Fig. 4 we plot $KC_s'^3/A^2$ versus C_ϵ for all 27 data sets from our 7 different flows and find some compelling evidence that, indeed, C_ϵ is close to being proportional to $C_s'^3/A^2$. This approximate proportionality appears to hold universally, i.e., for all our Reynolds numbers and all our flows.

Based on the assumptions of large- and small-scale isotropy [required[1] for $\epsilon=15\nu\langle(du/dx)^2\rangle$], and of Gaussianity of and statistical independence between $u(x)$ and du/dx [sufficient requirements[8–11] for $n_s^{-1}(L/\eta_*)=B\lambda$ with $B=\pi$ and, therefore, $C=1$], the constant of proportionality in $C_\epsilon \propto C_s'^3/A^2$ is $K=(15\pi^2)^{3/2}\approx 1801.3$, i.e., $C_\epsilon=KC_s'^3/A^2$. However, the line $C_\epsilon=KC_s'^3/A^2$ is above our data in the left plot of Fig. 4 indicating that this constant of proportionality is actually an overestimate. The right plot of Fig. 4 makes this point even more clearly by presenting the data in a particularly unfavorable way; $C_\epsilon/(KC_s'^3/A^2)$ is indeed close to 1, in fact closer to 1.1, at the smaller values of Re_λ, and increases

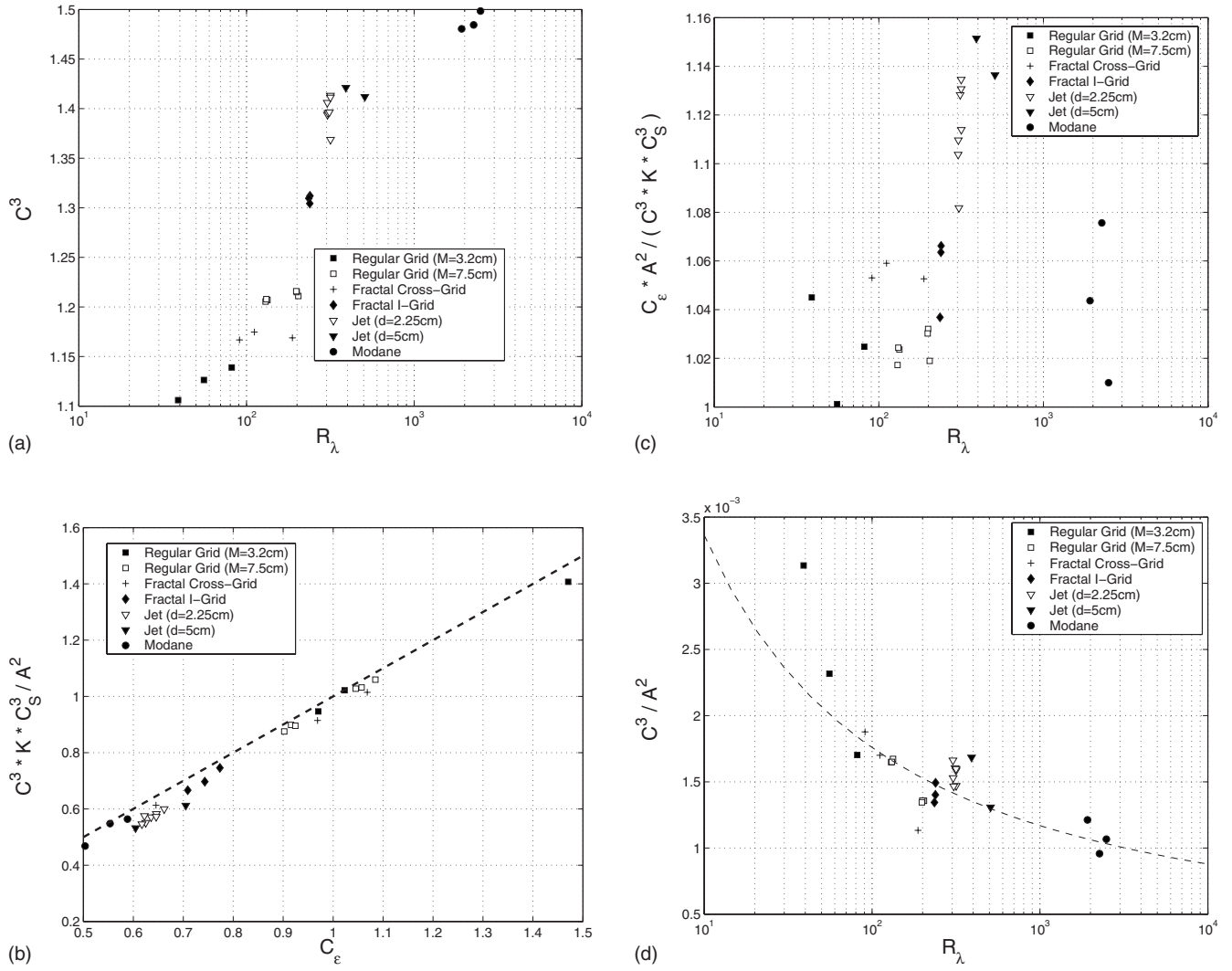

FIG. 5. Plots of C^3 vs $\log \mathrm{Re}_\lambda$, $C^3K(C_s'/A^{2/3})^3$ vs C_ϵ, $C_\epsilon/C^3K(C_s'/A^{2/3})^3$ vs $\log \mathrm{Re}_\lambda$ and C^3/A^2 vs $\log \mathrm{Re}_\lambda$. Explanations for how C, A and C_s' are calculated are given in the main text and the caption of Fig. 2. The dotted line in the second plot is $C^3K(C_s'/A^{2/3})^3=C_\epsilon$ and $K=(15\pi^2)^{3/2}\approx 1801.3$. The dotted curve in the fourth plot is $C^3/A^2\approx(0.87+0.11\log \mathrm{Re}_\lambda/7.8+9.1\log \mathrm{Re}_\lambda)^2$.

towards values above 1.6 with increasing Re_λ. Hence, there is a deviation from $C_\epsilon=KC_s'^3/A^2$ which increases systematically with increasing Reynolds number. Nevertheless, for the Reynolds numbers considered, $C_\epsilon=KC_s'^3/A^2$ is not so far from the data. This proximity to the data is surprising because of the different degrees of nonisotropy, non-Gaussianity and statistical dependence across scales in each one of the data sets. Each one of these data sets corresponds to a different location and/or a different Reynolds number in one of 7 different turbulent flows.

Of all the assumptions which together lead to $C_\epsilon=KC_s'^3/A^2$ we home in on the non-Gaussianity of du/dx as the weakest of them all. Relaxing this assumption does not invalidate Eq. (2), but forces us to consider $B\neq\pi$, and therefore $C_\epsilon=K(CC_s'/A^{2/3})^3$ with $C\equiv B/\pi\neq 1$. As explained by Liepmann and Robinson[8–11] and in the Appendix, this constant $C=B/\pi$ controls, in fact, the difference between $\langle|du/dx|\rangle$ and $\langle(du/dx)^2\rangle^{1/2}$: $C\langle|du/dx|\rangle=\sqrt{2/\pi}\langle(du/dx)^2\rangle^{1/2}$ and $C=1$ if du/dx is Gaussian. We have calculated $\langle|du/dx|\rangle$ and $\langle(du/dx)^2\rangle^{1/2}$ for all our data sets and plot the resulting values of C^3 as a function of $\log \mathrm{Re}_\lambda$ in Fig. 5. The derivative du/dx may be close to Gaussian at our lowest Reynolds numbers because C^3 is under 1.15 there, but becomes increasingly and systematically non-Gaussian as the Reynolds number increases. The increase of C^3 with $\log \mathrm{Re}_\lambda$ matches that of $C_\epsilon/K(C_s'/A^{2/3})^3$ in Fig. 4. As a result, $C_\epsilon=K(CC_s'/A^{2/3})^3$ fits the data much better than $C_\epsilon=K(C_s'/A^{2/3})^3$ (compare Figs. 5 and 4). We may claim that the relation $C_\epsilon=K(CC_s'/A^{2/3})^3$ is universal but we stress the need to try it on yet more turbulent flows, such as turbulent boundary layers and homogeneous shear flows, before such a claim may be cemented.

As shown in the last plot of Fig. 5, there remain some deviations to Eq. (2) which are all below 16% of $C_\epsilon/K(CC_s'/A^{2/3})^3=1$. These deviations are all such that $C_\epsilon/K(CC_s'/A^{2/3})^3$ is slightly larger than 1 and may be caused by our imperfect estimation of η_* and the fact that our calculation of C_s' from $n_s(L/\eta_c)L(L/\eta_c)^{2/3}$ with $\eta_c=\eta_*$ (rather than some other value of η_c between η_* and L) does, in fact, systematically underestimate C_s'. However, contributions to

these deviations may also come from the remaining nonuniversal factors such as differing degrees of anisotropy, and perhaps even slight non-Gaussian statistics of the large scales and slight statistical dependencies between large and small scales. It is surprising that these remaining factors may account, if they do, for so little of the nonuniversal behavior of C_ϵ most of which is caused by the universal strong dependence of C_ϵ on C_s', i.e., $C_\epsilon \sim C_s'^3$, and the nonuniversality of $C_s'^3$ which characterizes, in some sense, the number of large-scale eddies, i.e., the topology or topography of the large scales of the turbulence.

The Reynolds number dependence of C_ϵ results from the slow growth (with Reynolds number) of the range of viscous scales of the turbulence, i.e., on $A = \eta_* / \eta \approx 7.8 + 9.1 \log \mathrm{Re}_\lambda$, and from the slow increase (with Reynolds number) of the non-Gaussianity of the small scales, i.e., $C^3 \approx (0.87 + 0.11 \log \mathrm{Re}_\lambda)^2$ from an approximate fit of the first plot in Fig. 5. Just for the sake of keeping with tradition, and therefore rather arbitrarily, this type of fit has been chosen such that the Reynolds number dependence of C_ϵ, which is all in C^3/A^2 because of $C_\epsilon = K(CC_s'/A^{2/3})^3$, tends to a constant as $\mathrm{Re}_\lambda \to \infty$ (this is an assumption, usually accepted, but an assumption nonetheless). This constant turns out to be approximately 1.46×10^{-4}. Hence, in the limit where $\log \mathrm{Re}_\lambda \gg 1$,

$$C_\epsilon \approx \frac{1.46(15\pi^2)^{3/2}}{10^4} C_s'^3 \approx 0.26 C_s'^3, \tag{3}$$

if the assumption is made that our fits for the Reynolds number dependencies of C^3 and A can be extrapolated as $\log \mathrm{Re}_\lambda \to \infty$. [Fits of the dependencies of A and $C^{3/2}$ on Re_λ with functional forms such as $a_1(1 + a_2 \mathrm{Re}_\lambda^b)$ are also possible in principle with both positive and negative exponents b. In the case of positive exponents b, the requirement that C_ϵ should be finite in the limit $\mathrm{Re}_\lambda \to \infty$ forces the same exponent b in the fits of both $A = A(\mathrm{Re}_\lambda)$ and $C^{3/2} = C^{3/2}(\mathrm{Re}_\lambda)$. The requirement that C should grow indefinitely with Re_λ imposes a positive value of b which leads to fits of significantly lesser quality than our logarithmic fits.]

The formula $C_\epsilon \approx 0.26 C_s'^3$ predicts asymptotic constant values of C_ϵ about seven to eight times smaller than the usually accepted values which cluster near 0.5 (see the values of $C_s'^3$ in Fig. 2). The fit $C^3/A^2 \approx (0.87 + 0.11 \log \mathrm{Re}_\lambda / 7.8 + 9.1 \log \mathrm{Re}_\lambda)^2$ does reproduce values of C_ϵ close to the usual 0.5 for $\mathrm{Re}_\lambda \approx 2000$, which is the largest in this paper and of the same order as the largest ever tried. In the fourth plot of Fig. 5 we confirm the fit $C^3/A^2 \approx (0.87 + 0.11 \log \mathrm{Re}_\lambda / 7.8 + 9.1 \log \mathrm{Re}_\lambda)^2$. The relation (3) is an asymptotic extrapolation of this fit for very high values of $\log \mathrm{Re}_\lambda$. Measurements up to values of Re_λ as high as 10^9 are required to confirm that the asymptotic values of C_ϵ are indeed seven to eight times smaller than currently thought and that the logarithmic fits on which these extrapolations are based are indeed accurate enough.

We stress that most of the Reynolds number dependence of C_ϵ at small to moderate values of $\log \mathrm{Re}_\lambda$ comes from $A = \eta_* / \eta = 7.8 + 9.1 \log \mathrm{Re}_\lambda$, but the non-Gaussianity of du/dx catches up as $\log \mathrm{Re}_\lambda$ increases bringing in its own weaker Reynolds number dependence of C which can in principle eventually compensate that of A. The fit $C^{3/2} \approx 0.87 + 0.11 \log \mathrm{Re}_\lambda$ has been chosen so as to achieve such compensation.

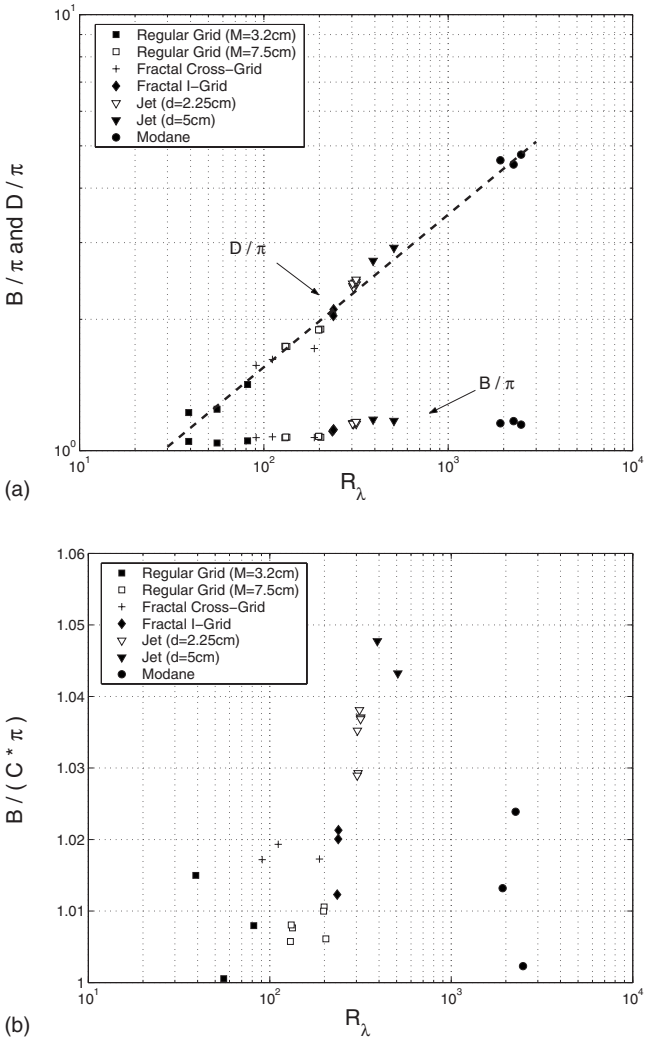

FIG. 6. Log-log plots of B/π and D/π vs Re_λ and lin-log plot of $B/(C\pi)$ vs Re_λ.

As a final note, it may be worth pointing out that there have been previous measurements[12] of B via independent estimations of $\bar{l}$ and λ and use of the Rice–Liepmann relation,[8–11] $\bar{l} = B\lambda$. In agreement with these measurements we find that B has a weak dependence on Reynolds number and on type of turbulent flow (see Fig. 6). In addition to these measurements we also estimate $\lambda_v \equiv \langle (l - \bar{l})^2 \rangle^{1/2}$, where l is the distance between consecutive zero-crossings and define the dimensionless constant D by $\lambda_v = D\lambda$. This length scale, which we call voids length scale, may be interpreted as characterizing the nonuniformity in the spatial distribution of zero-crossings and we find $D \sim \mathrm{Re}_\lambda^{1/3}$ (see Fig. 6). The weak dependence of B on Re_λ can be accounted for by $B = C\pi$ and the weak dependence on Re_λ of C calculated as for Fig. 5. This is confirmed in the second plot of Fig. 6.

III. MAIN CONCLUSIONS

The gist of our conclusions can be summarized as follows: a self-similar pattern is one where the small number of large scales is directly reflected in the large number of small scales. Zero-crossings of turbulent velocity fluctuations form such a pattern because of Eq. (1) and as a result, the average distance $\bar{l}$ between consecutive zero-crossings is strongly influenced by C_s' which is some sort of number of large-scale eddies within an integral scale. This average distance is proportional to the Taylor microscale λ (an explanation of this statement is given in the Appendix). Hence, the number of large-scale eddies directly affects the dimensionless dissipation rate C_ϵ: $C_\epsilon \propto C_s'^3$. This might be the physical-space equivalent of the Fourier-space effect recently reported by Bos *et al.*[21] who found numerically that C_ϵ depends on the structure of the small-wavenumber distribution and on the presence or absence of forcing at those wavenumbers.

It also turns out from our data analysis that the constant of proportionality relating $\bar{l}$ to λ depends on the deviations from Gaussianity of the statistics of du/dx. These deviations turn out to increase only logarithmically with Re_λ, and one of the central results of this paper is that

$$C_\epsilon = f(\log \mathrm{Re}_\lambda) C_s'^3. \tag{4}$$

The dimensionless function $f(\log \mathrm{Re}_\lambda)$ tends to 0.26 in the limit $\log \mathrm{Re}_\lambda \gg 1$ if the assumption is made that C_ϵ is finite in such a limit. This finite limit can be achieved by an eventual balance between the slow growth of the range of viscous scales and the slow increase in the non-Gaussianity of the small scales. We find that $f(\log \mathrm{Re}_\lambda) \approx 1801.3(0.87 + 0.11 \log \mathrm{Re}_\lambda / 7.8 + 9.1 \log \mathrm{Re}_\lambda)^2$. The numerator quantifies the increasing non-Gaussianity of the small scales and the denominator quantifies the slow increase of the range of viscous scales of the turbulence: $\eta_* = \eta(7.8 + 9.1 \log \mathrm{Re}_\lambda)$.

The natural length-scales to introduce in addition to the first moment $\bar{l}$ are the higher moments $\langle (l-\bar{l})^n \rangle^{1/n}$ for $n = 2, 3, \ldots$. We have ended this paper's investigation with a note concerning $n=2$, i.e., $\lambda_v \equiv \langle (l-\bar{l})^2 \rangle^{1/2}$. This length scale characterizes the nonuniformity in the spatial distribution of zero-crossings and we therefore call it the voids length scale. Future work on zero-crossings of turbulence signals should address all these length-scales and attempt to explain why λ_v scales with Reynolds number like none of the other known length scales of turbulence.

ACKNOWLEDGMENTS

We are grateful to Christophe Baudet, Yves Malecot, and Yves Gagne for providing us with their data.

APPENDIX: THE RICE THEOREM

To start understanding the proportionality between the average distance $\bar{l}$ between zero crossings of a random continuous function $u(x)$ and the Taylor microscale $\lambda = \langle u^2 \rangle^{1/2} / \langle (du/dx)^2 \rangle^{1/2}$, consider first the special case of an on-off telegraph signal $\tau(x)$. The number of discontinuities, and therefore zero-crossings, in this signal is equal to $\int |d\tau/dx| dx$ which means that the average distance between zero-crossings is proportional to the inverse of $\langle |d\tau/dx| \rangle$.

Now consider a random continuous function $u(x)$ such that $\int u(x) dx = 0$, and the resulting telegraph signal $H[u(x)]$, where the function $H(y)$ equals 1 for $y > 0$, 0 for $y = 0$ and -1 for $y < 0$. The number of zero-crossings in the random signal $u(x)$ is equal to the number of discontinuities of $H[u(x)]$ which is equal to $\int |d/dx H[u(x)]| dx$ which, in turn, equals $\int \delta[u(x)] |du/dx| dx$ in terms of the Dirac delta function. Assuming ergodicity and using the notation $v \equiv du/dx$ and $P(u,v)$ for the joint probability density function of u and v, it then follows that

$$1/\bar{l} = \int P(u,v) \delta(u) |v| du dv.$$

Restricting ourselves to cases where u and v are statistically independent, we obtain

$$1/\bar{l} = \langle |v| \rangle p(u=0) = \left\langle \left| \frac{du}{dx} \right| \right\rangle p(u=0),$$

where $p(u)$ is the probability density function of u. If u is statistically Gaussian, then $\sqrt{2\pi} \langle u^2 \rangle^{1/2} p(u=0) = 1$, and

$$\bar{l} = \frac{1}{\left\langle \left| \frac{du}{dx} \right| \right\rangle p(u=0)} = \sqrt{2\pi} \frac{\langle u^2 \rangle^{1/2}}{\left\langle \left| \frac{du}{dx} \right| \right\rangle}.$$

If du/dx is also statistically Gaussian with zero mean, then $\langle |du/dx| \rangle = \sqrt{2/\pi} \langle (du/dx)^2 \rangle^{1/2}$, thus yielding the Rice result[8,9]

$$\bar{l} = \pi \frac{\langle u^2 \rangle^{1/2}}{\left\langle \left(\frac{du}{dx} \right)^2 \right\rangle^{1/2}}.$$

In the case where $u(x)$ is assumed to be a turbulent fluctuation velocity component, du/dx is not Gaussian and $C \langle |du/dx| \rangle = \sqrt{2/\pi} \langle (du/dx)^2 \rangle^{1/2}$, where C is, in principle, different from 1. From such considerations, Liepmann[10,11] deduced the following relation between $\bar{l}$ and the Taylor microscale λ:

$$\bar{l} = B\lambda,$$

where $B = C\pi$. As shown in the present paper, deviations from $C=1$ in turbulence, i.e., from $\langle |du/dx| \rangle = \sqrt{2/\pi} \langle (du/dx)^2 \rangle^{1/2}$, turn out to be relatively small and grow with Reynolds number very slowly, in fact logarithmically.

[1] G. I. Taylor, "Statistical theory of turbulence," Proc. R. Soc. London, Ser. A **151**, 421 (1935).
[2] G. K. Batchelor, *The Theory of Homogeneous Turbulence* (Cambridge University Press, Cambridge, 1953).
[3] K. R. Sreenivasan, "On the scaling of the energy dissipation rate," Phys. Fluids **27**, 1048 (1984).
[4] K. R. Sreenivasan, "An update on the energy dissipation rate in isotropic turbulence," Phys. Fluids **10**, 528 (1998).
[5] Y. Kaneda, T. Ishihara, M. Yokokawa, K. Itakura, and A. Uno, "Energy dissipation rate and energy spectrum in high resolution direct numerical simulations of turbulence in a periodic box," Phys. Fluids **15**, L21 (2003).
[6] B. R. Pearson, T. A. Yousef, N. E. L. Haugen, A. Brandenburg, and P.-A.

Krogstad, "The 'zeroth-law' of turbulence in steady isotropic," 15th Australasian Fluid Mechanics Conference, The University of Sydney, Sydney, Australia, 13–17 December 2004.
[7]P. Burattini, P. Lavoie, and R. A. Antonia, "On the normalized turbulent energy dissipation rate," Phys. Fluids **17**, 098103 (2005).
[8]S. O. Rice, "Mathematical analysis of random noise," Bell Syst. Tech. J. **23**, 282 (1944).
[9]S. O. Rice, "Mathematical analysis of random noise," Bell Syst. Tech. J. **24**, 46 (1945).
[10]H. W. Liepmann, "Die anwendung eines satzes uber die nullstellen stochastischer funktionen auf turbulenzmessungen," Helv. Phys. Acta **22**, 119 (1949).
[11]H. W. Liepmann and M. S. Robinson, "Counting methods and equipment for mean-value measurements in turbulence research," NACA TN (1952), p. 3037.
[12]K. R. Sreenivasan, A. Prabhu, and R. Narasimha, "Zero-crossings in turbulent signals," J. Fluid Mech. **137**, 251 (1983).
[13]K. R. Sreenivasan, "Fractals and multifractals in fluid turbulence," Annu. Rev. Fluid Mech. **23**, 539 (1991).
[14]J. Davila and J. C. Vassilicos, "Richardson's pair diffusion and the stagnation point structure of turbulence," Phys. Rev. Lett. **91**, 144501 (2003).
[15]S. Orey, "Gaussian sample functions and the Hausdorff dimension of level crossings," Z. Wahrscheinlichkeitstheor. Verwandte Geb. **15**, 249 (1970).
[16]D. Hurst and J. C. Vassilicos, "Scalings and decay of fractal-generated turbulence," Phys. Fluids **19**, 035103 (2007).
[17]N. Mazellier, "Dynamique spatio-temporelle du champ de vorticité en turbulence." Ph.D. thesis, Universite Joseph Fourier, Grenoble, France (2005). Downloadable from http://tel.archives-ouvertes.fr/tel-00011427
[18]C. Baudet and R. H. Hernandez, "Spatial enstrophy spectrum in a fully turbulent jet," in *Advances in Turbulence VI*, edited by S. Gavrilakis, L. Machiels, and P. A. Monkewitz (Kluwer Academic, Dordrecht, 1996).
[19]H. Kahalerras, Y. Malecot, Y. Gagne, and B. Castaing, "Intermittency and Reynolds number," Phys. Fluids **10**, 910 (1998).
[20]Y. Malecot, C. Auriault, H. Kahalerras, Y. Gagne, O. Chanal, B. Chabaud, and B. Castaing, "A statistical estimator of turbulence intermittency in physical and numerical experiments," Eur. Phys. J. B **16**, 549 (2000).
[21]W. J. T. Bos, L. Shao, and J.-P. Bertoglio, "Spectral imbalance and the normalized dissipation rate of turbulence," Phys. Fluids **19**, 045101 (2007).